Available online at www.sciencedirect.com
SCIENCE DIRECT®
International Journal of Heat and Mass Transfer 49 (2006) 3448–3461
International Journal of HEAT and MASS TRANSFER
www.elsevier.com/locate/ijhmt

The thermagoustic irreversibility for a single-plate thermoacoustic system

Shohel Mahmud *, Roydon Andrew Fraser

Department of Mechanical Engineering, University of Waterloo, 200 University Avenue West, Waterloo, Ont., Canada N2L3G1

Received 13 May 2005; received in revised form 28 February 2006
Available online 18 May 2006

Abstract

The problem of thermagoustic (*ther*mo-*mag*neto-ac*oustic*) irreversibility near a single-plate, representative of the stack in a thermoacoustic engine, is modeled and analyzed in this paper. Assumptions (long wave, short stack, small amplitude oscillation, boundary layer type flow, etc.) are made to enable simplification of the governing continuity, momentum, and energy equations to achieve analytical solutions for velocity, temperature, and pressure. A general equation for entropy generation is derived from first principles that accounts for the transverse magnetic force present in a magnetohydrodynamic system. This entropy generation equation is then simplified in order to model the specific thermoacoustic situation considered in this paper. Finally, a time-averaged entropy generation rate followed by a global entropy generation rate are calculated and graphically presented for further analysis.

Keywords: Entropy; Global irreversibility; Magnetohydrodynamic; Thermoacoustics

1. Introduction

Thermoacoustic interactions, the interaction between acoustic waves and temperature oscillations, is a phenomenon present in acoustic boundary layers near rigid walls. Thermoacoustics can be simplistically defined as the physics of the interaction between thermal and acoustic fields, especially when one field gives rise to a significant gradient in the other field. A more careful description can be found in the general review article by Rott [1] in which thermoacoustics can be broadly classified into two main branches on the basis of cause and effect, namely: (1) time-averaged thermal/temperature-gradients driven fluid oscillations (Effect-A) and (2) time-averaged thermal/temperature-gradients induced by fluid oscillations (Effect-B).

Swift [2] identifies the former effect (Effect-A) as an effect similar to that seen in a conventional prime mover or engine and the latter effect (Effect-B) as an effect similar to that seen in conventional heat pump. The Effect-A includes, among the other issues, the vast body of work on Rijke (and related) tubes (see for example, Feldman [3]) and has received considerably far more attention than Effect-B. Efforts have been given to develop theories describing Effect-A. Even some early studies by Kirchhoff [4] and Rayleigh [5] indicate discussions about the production of sound from temperature gradients. However, Effect-B is a very recent issue and with most of the fundamental works conducted by Rott [1] and Swift [2].

Conventional engines and refrigerators have crankshaft-coupled pistons or rotating turbines. Thermoacoustic engines and refrigerators have at most a single flexing moving part (a loudspeaker) with no sliding seals. A thermoacoustic engine, whether it is a heat pump or prime mover, consists of four basic parts; specifically (a) a speaker, (b) a resonant tube, (c) a heat exchanger, and (d) a stack. The stack serves as the 'heart' of any thermoacoustic device and plays a key role in the operation of such devices. Positioned between the hot and cold heat exchangers, the stack determines how much and in what direction heat and work transfer will occur. Thermoacoustic devices

* Corresponding author. Tel.: +1 519 888 4567x3885.
E-mail address: shohel_mah@yahoo.ca (S. Mahmud).

0017-9310/$ - see front matter © 2006 Elsevier Ltd. All rights reserved.
doi:10.1016/j.ijheatmasstransfer.2006.02.051

Nomenclature

B	magnetic induction (Wb m^{-2})
Be	Bejan number, $(=Ns_{HT}/Ns_{tav})$
C_p	specific heat of the fluid at constant pressure (J kg^{-1} K^{-1})
C_v	specific heat of the fluid at constant volume (J kg^{-1} K^{-1})
DR	drive ratio $(=P_A/p_m)$
E	electrical field intensity (V m^{-1})
F	frequency of oscillation (Hz)
GFFI	global fluid friction irreversibility $(Ns_{av})_{FF}$
GHTI	global heat transfer irreversibility $(Ns_{av})_{HT}$
GMRI	global magneto-resistive irreversibility $(Ns_{av})_{MT}$
Ha_δ	Hartmann number $(B_y\delta_v\sqrt{\sigma/\mu})$
i	complex number $(\sqrt{-1})$
J	current density (amp m^{-2})
k_f	thermal conductivity of the fluid (W m^{-1} K^{-1})
Ns	entropy generation number
Ns_{FF}	time-averaged entropy generation due to fluid friction
Ns_{HT}	time-averaged entropy generation due to heat transfer
Ns_{MT}	time-averaged entropy generation due to magnetic dissipation
Ns_{tav}	time-averaged entropy generation number
P	pressure (N m^{-2})
P_A	amplitude of the fluctuating pressure (N m^{-2})
Pr	Prandtl number of the fluid $(=\delta_v^2/\delta_k^2)$
Re_m	magnetic Reynolds number $(=\mu_0\sigma u_0\delta)$
$\dot{S}_{gen}$	volumetric entropy generation rate (W m^{-3} K^{-1})
$\dot{s}_{gen}$	second-order simplification of the volumetric entropy generation rate, see Eq. (25)
T	temperature of the fluid (K)
T_{ad}	fluctuating temperature due to an adiabatic oscillation $(=T_m\beta p_1/\rho_m C_p)$
T_{sw}	standing wave temperature oscillation $(=\nabla T_m\nabla p_1/\rho_m\omega^2)$
u	axial velocity component (m s^{-1})
V	velocity vector (m s^{-1})

Greek symbols

α_f	thermal diffusivity of the fluid (m^2 s^{-1})
β	thermal expansion coefficient (K^{-1})
δ_v	viscous penetration depth $(=\sqrt{2\nu/\omega})$
δ_k	thermal penetration depth $(=\sqrt{2\alpha_f/\omega})$
μ	dynamic viscosity of the fluid (N m^{-2} s)
μ_0	permeability of the free space $(4\pi\times10^{-7}$ Wb amp^{-1} $m^{-1})$
ν	kinematic viscosity (m^2 s^{-1})
σ	electrical conductivity of the fluid (Ω^{-1} m^{-1})
ω	circular frequency (rad. s^{-1})
ρ	density of the fluid (kg m^{-3})
τ	time period $(2\pi/\omega)$
Φ	any variable, for example, u, T, p, etc.
λ	wavelength (m)

Subscripts and Superscripts

0	reference value
1	first-order variable
∞	free stream value
m	mean value
r	reference value
FF	fluid friction
HT	heat transfer
MT	magneto-thermoacoustic

Symbols

$\Re[\ ]$	real part of an expression
$\Im[\ ]$	imaginary part of an expression
$\overline{\Gamma}$	time-average of a complex expression Γ $(=\tau^{-1}\int_0^\tau \Gamma dt)$
$\langle\Gamma\rangle$	space integration of a complex expression Γ $(=\lim_{Z\to\Pi}\int_0^Z \Gamma dt)$

may be of practical use where simplicity, reliability, or low cost is more important than obtaining the highest possible efficiency (one cannot say much more about their cost-competitiveness at this early stage). They can provide cooling or heating using environmentally benign gases. Despite recent developments (see Swift [6]) in thermoacoustic engines, there are many areas requiring further investigation in order to better predict their performance and to guide the future designs of thermoacoustic engines.

There are two standard approaches used to solve thermoacoustic problems: (a) the single-plate thermoacoustic (SPT) approach and (b) the multi-plate thermoacoustic (MPT) approach. Although the multi-plate thermoacoustic system better represents a practical version of a thermoacoustic engine, many physical processes can be well understood from analyzing a single-plate thermoacoustic system. The fluid dynamic analysis of a single-plate thermoacoustic system is limited to a boundary layer type of analysis because of the unbounded nature of the flow and thermal fields. The bounded flow and thermal fields of a multi-plate thermoacoustic system reveals, in many circumstances, that the transverse (normal to the plate) variation in parameters is limited to a very thin layer (viscous and thermal penetration depth) above and below the plate. Thermoacoustic effects exist only in this thin layer [1,2]. In such situations, one can also use a boundary layer approach for multi-plate thermoacoustic system similar to that used in a single-plate thermoacoustic system.

For a single plate thermoacoustic system, Swift [2] develops an inviscid standing wave model which is modi-

fied for a traveling wave by Raspet et al. [7]. Santillan and Boullosa [8,9] include the effect of viscosity to the single plate thermoacoustic model developed by Swift [2] and Raspet et al. [7]. Swift et al. [10] discuss the possibility of using liquid metals as working fluids in thermoacoustic engines which opens the door of possibly to using of magnetic force in thermoacoustics. Wheatley et al. [11] built a demonstration prime mover using liquid sodium. A prime use for Magnetic force is as a fluid oscillation and time phasing control mechanism in the vicinity of a thermoacoustic stack. In general, the action of a transverse magnetic force is similar to a drag force [12] imposed on a moving fluid. Another important application of combined thermoacoustics and magnetic force is found in magnetic refrigerators [13] in the form of the magnetocaloric effect. A recent study by Ibanez et al. [14] optimized the performance parameters of a magnetohydrodynamic generator and a study by Ovando et al. [15] is limited to an instability analysis.

In spite of the remarkable contributions by many researchers in developing thermoacoustic theories and improving thermoacoustic engine performance, poor efficiency is still the thermoacoustic engine's major weakness, and its inherent irreversibility is a major reason for this weakness. The major focuses of most published articles related to thermoacoustics are energy flux calculations [2], stability limit determination [1], heat exchangers' length optimization [16], etc. Only one article by Ishikawa and Mee [17] focuses on, and then only a little, the important issue of irreversibility in a multi-plate thermoacoustic system via entropy generation analysis. For a real system in a fixed environment the generated entropy is proportional to the destroyed exergy [18]. Exergy is always destroyed in the presence of irreversibilities, either partially or totally: this is a consequence of the Second-law of thermodynamics. The destroyed exergy, or the generated entropy, is responsible for the less-than-theoretical thermodynamic efficiency of any system. By performing exergy accounting in smaller and smaller subsystems (total system → components → elemental surfaces → differential levels), one is able to draw a map of how the exergy destruction is distributed over the engineering system of interest [19]. In this way, one is able to pinpoint the components and mechanisms (processes) that destroy the most exergy. This is a real advantage in the search to improve efficiency, because it tells us from the start how to allocate engineering effort and resources. The beauty of an exergy-based analysis is that it makes it possible to compare on a common basis (entropy generation platform) different interactions (inputs, outputs, work transfer, heat transfer, etc.) in a system, and enables minimization of the global entropy generation rate (entropy generation minimization or EGM).

In the view of the above observations, the objective of this study is to examine the nature of the irreversibility found in a single plate thermoacoustic system in the presence of a transverse magnetic field. Entropy generation rate is used as the measure of irreversibility.

2. Problem formulation

The continuity, Navier-Stokes, and energy equations are used to describe the effects of a plane standing acoustic wave whose direction of oscillation is aligned with the axis of the plane-parallel geometry of a single plate as shown in Fig. 1. The single plate in Fig. 1 is the typical configuration representative of the thermoacoustic engine stack.

The electromagnetic field cannot create mass, and the continuity equation remains unchanged [20] in the following form:

$$\frac{D\rho}{Dt} + \rho \mathrm{div}(\mathbf{V}) = 0, \tag{1}$$

where $\mathbf{V}$ is the velocity vector. Considering only the electromagnetic force as a source term, one can write the momentum equation in a general form as

$$\rho \frac{D\mathbf{V}}{Dt} = -\nabla p + \mu \nabla^2 \mathbf{V} + \mathbf{F}_{\mathrm{em}}, \tag{2}$$

where $\mathbf{F}_{\mathrm{em}}$ represents the electromagnetic force. The electromagnetic volume force ($\mathbf{F}_{\mathrm{em}}$) acts as a ponderomotive (where the fluid is considered a rigid current carrier moving in a magnetic field) force [21] and can be estimated form

$$\mathbf{F}_{\mathrm{em}} = \mathbf{J} \times \mathbf{B}, \text{ where } \mathbf{J} = \sigma(\mathbf{E} + \mathbf{V} \times \mathbf{B}), \tag{3}$$

part of which would exist if the fluid were at rest, and part of which is due to the current induced by fluid motion through the magnetic field. In Eq. (3), $\mathbf{J}$, $\mathbf{B}$, σ, and $\mathbf{E}$ are the volume current density, magnetic induction, electrical conductivity of the fluid, and electric field intensity, respectively. The force $\sigma(\mathbf{E} \times \mathbf{B})$ accelerates or decelerates the flow, depending on the direction of $\mathbf{E}$, $\mathbf{B}$, and $\mathbf{V}$; the back electromagnetic force or emf $\sigma(\mathbf{V} \times \mathbf{B})$ provides a current whose interaction with $\mathbf{B}$ always decelerates the flow.

The interaction of magnetic force in the energy equation appears as volumetric rate of electrical dissipation work (Joule heating) in a conductor [21,22]. Now, considering Joule heating, the general form of energy equation becomes

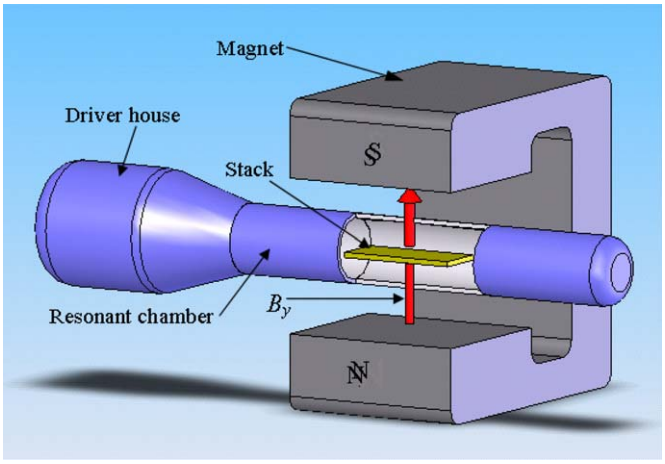

Fig. 1a. A 3D view of the considered problem.

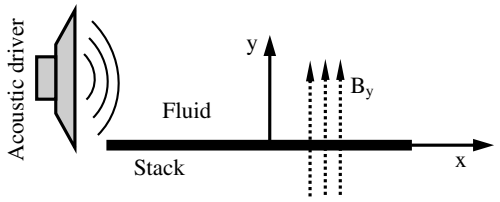

Fig. 1b. Schematic diagram of the problem under consideration.

$$\rho\frac{De_i}{Dt} = -\mathrm{div}(\mathbf{q}) - p\,\mathrm{div}(\mathbf{V}) + \mu\Phi + \sigma|\mathbf{E}+\mathbf{V}\times\mathbf{B}|^2. \tag{4}$$

where e_i is the internal energy, $\mathbf{q}$ is the heat flux vector, and Φ is the dissipation function, respectively. In a 2D Cartesian frame of reference Φ can be given by the following expression [20]:

$$\Phi = \left\{-\frac{2}{3}\left(\frac{\partial u}{\partial x}+\frac{\partial v}{\partial y}\right)^2 + 2\left(\frac{\partial u}{\partial x}\right)^2 + 2\left(\frac{\partial v}{\partial y}\right)^2 + \left(\frac{\partial v}{\partial x}+\frac{\partial u}{\partial y}\right)^2\right\}. \tag{5}$$

3. Equation of entropy generation

The aim of this section is to derive an equation for entropy generation from scratch that includes the influence of a magnetic field. We follow a procedure similar to that available in Bird et al. [20], Burmeister [23], and Bejan [24].

When a system is not in thermodynamic equilibrium, due to the existence of velocity and temperature gradients, strictly speaking, definitions of thermodynamic quantities are no longer meaningful. However, within a small volume of fluid, the thermodynamic state of the fluid inside the volume can be regarded as uniform and in local equilibrium [18]. When considering the entropy balance in the small volume, the volume entropy change should equal the sum of the net entropy flow that enters and the entropy generated within the volume [20]. As the volume approaches zero, the entropy balance can be expressed as follows:

$$\rho\frac{Ds}{Dt} = -\mathrm{div}(\dot{\mathbf{s}}) + \dot{S}_{\mathrm{gen}}, \tag{6}$$

where s is the entropy per unit mass, $\dot{\mathbf{s}}$ is the entropy flux vector, which is measured with respect to fluid velocity, and $\dot{S}_{\mathrm{gen}}$ is the rate of entropy generation per unit volume. Taking the substantial derivative of the canonical expression $de_i = Tds - pd(1/\rho)$ yields

$$T\frac{Ds}{Dt} = \frac{De_i}{Dt} - \frac{p}{\rho^2}\frac{D\rho}{Dt}. \tag{7}$$

The energy equation (Eq. (4)) and continuity equation (Eq. (1)) allow the first and second terms on the right-hand side of Eq. (7) to be expressed as

$$\frac{De_i}{Dt} = -\frac{\mathrm{div}(\mathbf{q})}{\rho} - \frac{p\,\mathrm{div}(\mathbf{V})}{\rho} + \frac{\mu\Phi}{\rho} + \frac{\sigma|\mathbf{E}+\mathbf{V}\times\mathbf{B}|^2}{\rho} \tag{8}$$

and

$$\frac{p}{\rho^2}\frac{D\rho}{Dt} = -\frac{p\,\mathrm{div}(\mathbf{V})}{\rho}, \tag{9}$$

respectively.

Substituting Eqs. (8) and (9) on the right-hand side of Eq. (7) yields

$$\rho\frac{Ds}{Dt} = -\frac{\mathrm{div}(\mathbf{q})}{T} + \frac{\mu\Phi}{T} + \frac{\sigma|\mathbf{E}+\mathbf{V}\times\mathbf{B}|^2}{T}. \tag{10}$$

Now, recall that the divergence of a scalar times a vector is

$$\mathrm{div}\left(\frac{\mathbf{q}}{T}\right) = \frac{\mathrm{div}(\mathbf{q})}{T} + \mathbf{q}.\nabla\left(\frac{1}{T}\right) = \frac{\mathrm{div}(\mathbf{q})}{T} - \frac{\mathbf{q}.\nabla T}{T^2}, \tag{11}$$

therefore, the substantial derivative of entropy (Eq. (10)) becomes

$$\rho\frac{Ds}{Dt} = -\mathrm{div}\left(\frac{\mathbf{q}}{T}\right) + \left(-\frac{\mathbf{q}.\nabla T}{T^2} + \frac{\mu\Phi}{T} + \frac{\sigma|\mathbf{E}+\mathbf{V}\times\mathbf{B}|^2}{T}\right). \tag{12}$$

Comparison of Eqs. (6) and (12) shows that the diffusive flux on entropy relative to bulk convection is given by

$$\dot{\mathbf{s}} = \frac{\mathbf{q}}{T} \tag{13}$$

and the volumetric rate of generation of entropy per unit mass is given by

$$\dot{S}_{\mathrm{gen}} = -\frac{\mathbf{q}.\nabla T}{T^2} + \frac{\mu\Phi}{T} + \frac{\sigma|\mathbf{E}+\mathbf{V}\times\mathbf{B}|^2}{T} \tag{14}$$

and further substituting $\mathbf{q} = -k\nabla T$ yields

$$\dot{S}_{\mathrm{gen}} = \left[\frac{k_f(\nabla T)^2}{T^2}\right] + \left[\frac{\mu\Phi}{T} + \frac{\sigma|\mathbf{E}+\mathbf{V}\times\mathbf{B}|^2}{T}\right]. \tag{15}$$

Eq. (15) is the general equation of volumetric entropy generation rate (W m^{-3} K^{-1}) in the presence of a magnetic force. A simplified form of Eq. (15) that is suitable for the present problem will be given later. Expressions of velocity and temperature are required in order to get an expression for the entropy generation from the simplified version of Eq. (15).

4. Flow and thermal fields

In this section, the expressions of velocity and temperature are derived after simplifying and solving the governing momentum and energy equations (Eqs. (2) and (4)). Although a specific form of the energy equation (Eq. (4)) is used to derive the entropy generation equation, this form is not suitable for analytical treatment to get an expression of temperature. The following full form of the energy equation:

$$\rho C_p\left[\frac{\partial T}{\partial t} + \mathbf{V}.\nabla T\right] = k_f\nabla^2 T + \beta T\frac{Dp}{Dt} + \sigma|\mathbf{E}+\mathbf{V}\times\mathbf{B}|^2 + \mu\Phi \tag{16}$$

is used in this section in the treatments that follows. In Eq. (16), C_p, k_f, and β are the specific heat of the fluid at

constant pressure, thermal conductivity of the fluid, and the volumetric thermal expansion coefficient, respectively. A magnetic force is assumed to act along the normal direction (here the y-axis) of the stack. In the initial quiescent state (in the absence of the acoustic field), at a mean pressure (p_m) and mean density (ρ_m) the fluid and stack are assumed to be isothermal at the quiescent temperature (T_m). The fluid is assumed to be at a motionless state; that is, $u_m = 0$ and $v_m = 0$. In the presence of the acoustic field, all variables have mean parts (for example, p_m, T_m, etc.) plus small amplitude oscillating parts (for example, $\hat{p}_1, \widehat{T}_1$, etc.). The oscillating part of any variable depends on both space (x and y) and time (t). Using Rott's [1] linear thermoacoustic approximation, one can split the oscillating part of a variable into a space dependent part (for example, p_1) multiplied by a time-dependent part ($\exp(i\omega t)$). The space dependent part of a variable is, in general, a complex expression reflecting the time phasing of the oscillating quantity.

A very low magnetic Reynolds number ($Re_m = \mu_0 \sigma u_0 \delta \ll 1$) is assumed because, in a typical thermoacoustic problem, the product of the characteristic length (δ) and permeability of free space (μ_0) are very small. It is also assumed that the flow is nearly unidirectional; that is, parallel to the direction of the stack. It is further assumed that an uniform, imposed magnetic field ($\mathbf{B} \approx B_y \hat{\mathbf{j}}$) acts parallel to the y-axis as shown in Fig. 1. When $Re_m \ll 1$, $\mathbf{B}$ influences $\mathbf{V}$ (via the Lorentz force), but $\mathbf{V}$ does not significantly perturb $\mathbf{B}$ [25]. Therefore, the induced magnetic field is negligible in comparison to the imposed field. We may also consider the magnetic field to be approximately equal to the imposed field when $Re_m \ll 1$. Since $\mathbf{B}$ is now almost constant, the electric field must be irrotational ($\nabla \times \mathbf{E} = 0$) and one can write $\mathbf{E} = -\nabla\varphi$, where φ is the electrostatic potential. Now, the divergence of electric field [25] leads to the following expression:

$$\nabla \cdot \mathbf{J} = -\sigma \nabla^2 \varphi + \sigma \nabla \cdot (B_y u \hat{\mathbf{k}}) = -\sigma \nabla^2 \varphi + \sigma B_y \frac{\partial u}{\partial z} = 0, \tag{17}$$

which yields $\nabla^2 \varphi = 0$. We also assume that there is no imposed electric field, and so $\varphi = 0$. Now the magnetic source term in Eqs. (2) and (3) reduces to

$$\mathrm{F}_{em} = (\mathbf{J} \times \mathbf{B}) = -\sigma u B_y^2 \hat{\mathbf{i}}. \tag{18}$$

Any variable Φ (where Φ stands for u, ρ, p, T, etc.) can be expanded [1,2] according to the following equation:

$$\Phi = \Phi_m + \widehat{\Phi}_1; \quad \text{where } \widehat{\Phi}_1 = \Phi_1 \mathrm{e}^{i\omega t}. \tag{19}$$

The term with subscript 'm' is the mean and with subscript '1' is the fluctuating part of that variable. The fluctuating part ($\widehat{\Phi}_1$) can be further expressed as a space dependent part (Φ_1) multiplied by a time-dependent part ($\exp(i\omega t)$) where ω represents the angular frequency which equals $2\pi f$ and f is the ordinary frequency. Now, substituting Eq. (19) into Eqs. (2), (18), and (16) and keeping only the first-order terms, one can obtain the simplified momentum equation as

$$\rho_m \frac{\partial \hat{u}_1}{\partial t} = -\frac{\partial \hat{p}_1}{\partial x} + \mu \frac{\partial^2 \hat{u}_1}{\partial y^2} - \sigma B_y^2 \hat{u}_1 \tag{20}$$

and the simplified energy equation as

$$\rho_m C_p \frac{\partial \widehat{T}_1}{\partial t} + \rho_m C_p \hat{u}_1 \frac{\partial T_m}{\partial x} = k_f \frac{\partial^2 \widehat{T}_1}{\partial y^2} + \beta T_m \frac{\partial \hat{p}_1}{\partial t}. \tag{21}$$

The following boundary conditions:

$$\begin{aligned} &\text{at } y = 0, \quad u_1 = 0 \text{ and } T_1 = 0, \\ &\text{at } y \to \infty, \quad u_1 \text{ and } T_1 \text{ are finite} \end{aligned} \tag{22}$$

are used to obtain analytical solutions to Eqs. (20) and (21). Note that for the first boundary condition for the fluctuating temperature ($T_1 = 0$), it is assumed that the plate has a large enough heat capacity per unit area that its temperature does not change appreciably at the acoustic frequency [2]. This is a very good approximation if one considers a non-conjugate problem or a very thin stack approximation.

Now, solving Eq. (20) in the frequency domain and applying the boundary condition for velocity (given by Eq. (22)), one obtains an expression for the fluctuating velocity as

$$u_1 = \frac{i}{\rho_m \omega (1 + Ha_\delta^2/2i)} \times \frac{\partial p_1}{\partial x} \left[1 - \exp\left\{ -(1+i)\sqrt{1 + \frac{Ha_\delta^2}{2i}} \frac{y}{\delta_v} \right\} \right], \tag{23}$$

where Ha_δ and δ_v are the Hartmann number ($B_y \delta_v \sqrt{\sigma/\mu}$) and viscous penetration depth ($\sqrt{2v/\omega}$), respectively. The square of the Hartmann number is the ratio of the ponderomotive force to the viscous force [26]. In Eq. (23), Hartmann number is calculated based on the length scale δ_v. Note that in the limit of very large transverse distance ($y \gg \delta_v$) the exponential term in Eq. (23) goes to zero; thus leading a constant free stream velocity ($u_{1,\infty}$) which equals the terms outside the square bracket of Eq. (23).

Now, solving Eq. (21) in the frequency domain and applying the boundary condition for temperature (given by Eq. (22)), one obtains, after a long calculation, an expression for the fluctuating temperature as

$$\begin{aligned} T_1 = &\left[\frac{\beta T_m p_1}{\rho_m C_p} - \frac{\nabla T_m \nabla p_1}{\omega^2 \rho_m (1 + Ha_\delta^2/2i)} \right] + \frac{\nabla T_m \nabla p_1}{\omega^2 \rho_m (1 + Ha_\delta^2/2i)} \\ &\times \frac{Pr}{Pr - (1 + Ha_\delta^2/2i)} \times \exp\left\{ -(1+i)\sqrt{1 + \frac{Ha_\delta^2}{2i}} \frac{y}{\delta_v} \right\} \\ &- \left[\frac{\beta T_m p_1}{\rho_m C_p} + \frac{\nabla T_m \nabla p_1}{\omega^2 \rho_m} \frac{1}{Pr - (1 + Ha_\delta^2/2i)} \right] \exp\left\{ -(1+i)\frac{y}{\delta_k} \right\} \end{aligned} \tag{24}$$

where δ_k and Pr is the thermal penetration depth ($\sqrt{2\alpha_f/\omega}$) and Prandtl number (δ_v^2/δ_k^2) of the fluid, respectively. Similar to the fluctuating velocity, the fluctuating temperature approaches a free stream temperature ($T_{1,\infty}$) in the limit of very large transverse distance. The free stream temperature ($T_{1,\infty}$) equals the terms inside the first square bracket on the right-hand side of Eq. (24). Note that the square root of the Prandtl number can be expressed as a ratio of the viscous penetration depth (δ_v) to the thermal penetration depth (δ_k).

5. Entropy generation

A simplification of Eq. (15) is required in order to obtain an expression for entropy generation rate. Using the same assumptions already applied to simplify the momentum and energy equations, the simplified version of the entropy generation equation is

$$\dot{s}_{\text{gen}} = \frac{k_f}{T_0^2}\left(\frac{\partial \widehat{T}_1}{\partial y}\right)^2 + \frac{\mu}{T_0}\left(\frac{\partial \hat{u}_1}{\partial y}\right)^2 + \frac{\sigma B_y^2}{T_0}\hat{u}_1^2. \tag{25}$$

Here, we further assume that the variation of the fluctuating temperature in the fluid region of the stack is small [18] compared to the absolute temperature, hence $T \approx T_0$ where T_0 is a characteristic (reference) absolute temperature. Instead of defining a new reference temperature, one may set $T_0 = T_m$ in order to keep the analysis manageable. Using the following characteristic entropy generation rate

$$\dot{s}_0 = \frac{k_f}{\delta_v^2} = \frac{k_f}{Pr\delta_k^2} \tag{26}$$

it is possible to convert Eq. (25) into non-dimensional form as

$$Ns = \left[\left(\frac{\delta_v}{T_m}\right)^2\left(\frac{\partial \widehat{T}_1}{\partial y}\right)^2\right] + \left[\left(\frac{\mu}{T_m k_f}\right)\left\{\delta_v^2\left(\frac{\partial \hat{u}_1}{\partial y}\right)^2 + Ha_\delta^2\hat{u}_1^2\right\}\right], \tag{27}$$

where Ns is the entropy generation number [27] which is a dimensionless measure of the entropy generation rate ($\dot{s}_{\text{gen}}$). The definition of $\dot{s}_0$ depends on the specific type of problem. More discussions about $\dot{s}_0$ are available in Bejan [18] and Mahmud and Fraser [27]. The first square bracketed terms on the right-hand side of Eq. (27) represent the heat transfer contribution to entropy generation and the second square bracketed terms represent the fluid flow contribution to entropy generation. The fluid flow contribution is further divided into two parts: (1) fluid friction contribution which is proportional to the square of the velocity gradient and (2) magnetic force contribution which is proportional to the square of the fluctuating velocity times Hartmann number. The common term, $\mu/T_m k_f$, is actually the inverse of a characteristic velocity square because

$$u_0 = \sqrt{\frac{k_f T_m}{\mu}} \sim \left[\frac{\text{unit of length}}{\text{unit of time}}\right]. \tag{28}$$

By substituting Eqs. (23) and (24) into Eq. (27) and recalling the relation given in Eq. (19), one obtains a general form of entropy generation equation for a single-plate thermoacoustic system in the presence of a transverse magnetic field which is, of course, a function of time and space. However, our main intention is to obtain a time-averaged and then a global entropy generation rate in order to reduce the number of parameters on which entropy generation rate depends. Both time-averaged and global entropy generation rates have more practical physical meanings and applications. The time averaging technique [28] of the product of two complex quantities (for example, $\widehat{\Phi}_1\widehat{\Psi}_1$) can be expressed as

$$\overline{\widehat{\Phi}_1\widehat{\Psi}_1} = \frac{1}{\tau}\int_0^\tau \Re[\widehat{\Phi}_1]\Re[\widehat{\Psi}_1]\mathrm{d}t = \frac{1}{2}\Re[\Phi_1\widetilde{\Psi}_1] = \frac{1}{2}\Re[\widetilde{\Phi}_1\Psi_1], \tag{29}$$

where '$\Re[\ ]$' signifies the real part of a complex quantity and the tilde ($\sim$) denotes the complex conjugate. In Eq. (29), τ ($=2\pi/\omega$) is the period of oscillation. In this paper, we prefer an over bar ($\bar{}$) to specify the time-average of a certain quantity/quantities. When $\widehat{\Phi}_1 = \widehat{\Psi}_1$, Eq. (29) reduces to a special form given by

$$\overline{\widehat{\Phi}_1\widehat{\Phi}_1} = \frac{1}{\tau}\int_0^\tau (\widehat{\Phi}_1\widehat{\Phi}_1)\mathrm{d}t = \frac{1}{2}\Re[\Phi_1\widetilde{\Phi}_1] = \frac{1}{2}|\Phi_1|^2, \tag{30}$$

where '$|\ |$' denotes the absolute value of a complex quantity. Eq. (30) is applied to obtain the time-averaged entropy generation rate from Eq. (27) as

$$Ns_{\text{tav}} = \frac{\delta_v^2}{2T_m^2}\left|\frac{\partial T_1}{\partial y}\right|^2 + \left(\frac{\mu}{2T_m k_f}\right)\left\{\delta_v^2\left|\frac{\partial u_1}{\partial y}\right|^2 + Ha_\delta^2|u_1|^2\right\}. \tag{31}$$

The concept of spatial averaging any quantity that extends theoretically from zero to infinity can lead to interpretation difficulties. One encounters such a problem in the single-plate thermoacoustic system due to its unbounded nature in the transverse direction. However, a multi-plate thermoacoustic system is free from such a problem due to its finite transverse dimension. Instead of calculating a space-averaged entropy generation rate we prefer to calculate the global (or total) value of entropy generation rate from its time-averaged value. The following expression:

$$\langle\overline{\widehat{\Phi}_1\widehat{\Phi}_1}\rangle = \lim_{Z\to\Pi}\int_0^Z \frac{1}{\tau}\int_0^\tau (\widehat{\Phi}_1\widehat{\Phi}_1)\mathrm{d}t\,\mathrm{d}y = \frac{1}{2}\lim_{Z\to\Pi}\int_0^Z |\Phi_1|^2\mathrm{d}y \tag{32}$$

is used in order to obtain the global value of entropy generation. In Eq. (32), we chose the symbol '$\langle\ \rangle$' to represents a space integration and Π is a very large number with dimension of distance that may extend to infinity. The choice of the integration limit for spatial integration in

Eq. (32) requires further discussion; it is discussed later in this paper.

After performing time and space integrations of Eq. (27) it is possible to split the global entropy generation rate (Ns_{av}) in three terms as follows

$$Ns_{av} = (Ns_{av})_{HT} + (Ns_{av})_{FF} + (Ns_{av})_{MT} \tag{33}$$

for convenience and better interpretation. The first term on the right-hand side of Eq. (33) is the global heat transfer irreversibility (GHTI) and can be expressed as

$$(Ns_{av})_{HT} = \frac{1}{2}\left(\frac{\delta_v}{T_m^2}\right)\Re\left[\frac{b_1\tilde{b}_1 a_0\tilde{a}_0}{a_0+\tilde{a}_0}+\frac{b_2\tilde{b}_2 b_0\tilde{b}_0}{b_0+\tilde{b}_0}+\frac{b_1 a_0\tilde{b}_2\tilde{b}_0}{a_0+\tilde{b}_0}+\frac{b_2 b_0\tilde{b}_1\tilde{a}_0}{\tilde{a}_0+b_0}\right], \tag{34}$$

where tilde ($\sim$) denotes the complex conjugate as before. The definitions of a_0, $\tilde{a}_0$, b_0, $\tilde{b}_0$, b_1, $\tilde{b}_1$, b_2, and $\tilde{b}_2$ are given in Appendix. Note that a_0 and b_0 are equivalent to the inverse of some length scales (that is, penetration depths) and b_1 and b_2 represent temperature amplitude factors [29]. The second term on the right-hand side of Eq. (33) is the global fluid friction irreversibility (GFFI) and can be expressed as

$$(Ns_{av})_{FF} = \frac{\sqrt{4+Ha_\delta^4}}{\sqrt{2}}\frac{u_{1,\infty}\tilde{u}_{1,\infty}}{u_0^2} \times \Re\left[\frac{1}{(1+i)\sqrt{2-iHa_\delta^2}+(1-i)\sqrt{2+iHa_\delta^2}}\right], \tag{35}$$

and the last term on the right-hand side of Eq. (33) is the global magneto-resistive irreversibility (GMRI) and can be expressed as

$$(Ns_{av})_{MT} = \frac{Ha_\delta^2}{\sqrt{2}}\frac{u_{1,\infty}\tilde{u}_{1,\infty}}{u_0^2} \times \Re\left[\Pi^* - \frac{(4i+\sqrt{4+Ha_\delta^4})}{\sqrt{4+Ha_\delta^4}\{(1-i)\sqrt{2+iHa_\delta^2}+(1+i)\sqrt{2-iHa_\delta^2}\}}\right]. \tag{36}$$

Eqs. (23), (24), and (34)–(36) are the major findings of this paper. During spatial integration of Eq. (33) the application of the lower limit of y ($y = 0$) causes no problem. The application of the upper limit of y (y=$\Pi \to \infty$) to the y-dependent terms also causes no problem because y appears inside the negative exponential terms which go to zero when Π goes to infinity. However, an application of the upper limit of y to the y-independent terms requires additional discussion. Theoretically, the y-dependent part (when y appears inside negative exponential) of any expression (for example, Eqs. (23), (24) or (30)) goes to zero when y approaches a very large value ($\Pi \to \infty$). In reality, this large value of y is limited to a distance equal to a few penetration depths (δ_v and δ_k). For a single-plate inviscid oscillation, Swift [2] shows that the magnitude of Π equals 3–4 times the thermal penetration depth (δ_k). For the present problem we apply a series of different Π to the upper limit of y and carefully select a special $\Pi(=\Pi_0$ for example) that makes the y-dependent part almost equal to zero during the integration process. The three important parameters of GHTI, GFFI, and GMTI, are then calculated by setting the limit of y in Eq. (33) from 0 to Π^*, where Π^* is the non-dimensional value of Π_0.

6. Results and discussion

It is very difficult to interpret directly the different terms in Eqs. (23), (24), and (34)–(36). Instead, we quickly make some assumptions to simplify these equations for better interpretation. Note that the expressions already derived in the previous sections are complex in nature, only the real parts of these expressions have physical meanings.

6.1. Limiting cases of velocity and temperature

In the limit of large transverse distance the fluctuating velocity (Eq. (23)) changes to the y-independent free stream velocity ($u_{1,\infty}$) which is a function of mean density, frequency of oscillation, pressure gradient, and Hartmann number. An expression of $u_{1,\infty}$ is given in Appendix and is not repeated here. An increasing Hartmann number reduces the boundary layer thickness and in the limit of large Hartmann number the boundary layer thickness becomes zero. Similarly, in the limit of large transverse distance the fluctuating temperature (Eq. (24)) changes to the y-independent free stream temperature ($T_{1,\infty}$) which is a function of mean density, mean temperature, thermal expansion coefficient, frequency of oscillation, pressure gradient, temperature gradient, Prandtl number, and Hartmann number. An expression for $T_{1,\infty}$ is given in Appendix (Eq. (A1)) and is not repeated here. In the limit of large Hartmann number Eq. (24) reduces to an equation of the fluctuating temperature near a single plate for an inviscid oscillation [2]. When $Ha_\delta = 0$, Eq. (24) reduces to a form that is obtained by Santillan and Boullosa [9] with ε_s equal to zero, where ε_s is the fluid to solid heat capacity ratio [2] and is an important parameter for conjugate thermoacoustic problems.

6.2. Modeling of fluctuating pressure

To model pressure, one needs to construct a wave equation using the continuity and momentum equations, and thermodynamic relations. Modeling a wave equation depends on the specific type of thermoacoustic problem [1,2]. For the current problem, it is assumed that the stack is short enough that it does not perturb the standing wave appreciably (short stack approximation), so we may consider

$$p_1 = P_A \sin\left(\frac{x}{\tilde{\lambda}}\right) \text{ and } \frac{\partial p_1}{\partial x} = \frac{P_A}{\tilde{\lambda}}\cos\left(\frac{x}{\tilde{\lambda}}\right); \quad \text{where } \tilde{\lambda} = \frac{\lambda}{2\pi}. \tag{37}$$

In Eq. (37), λ is the wavelength and P_A is the amplitude of the fluctuating pressure which depends on the drive ratio DR ($=P_A/p_m$, $p_m=$ mean pressure). Drive ratio (DR) is a very important input parameter for thermoacoustic systems; it represents a measure of Mach number (Ma). If Mach number is defined as the ratio of the amplitude of the fluctuating velocity (u_a) to the velocity of sound (c_m) calculated at the mean fluid temperature (T_m), then the following expression

$$Ma=\frac{u_a}{c_m}=\frac{\mathrm{DR}}{\gamma} \tag{38}$$

is a relation between Mach number and drive ratio where γ is the specific heat ratio ($=C_p/C_v$) of the fluid.

6.3. Limiting cases of GHTI, GFFI, and GMRI

In this section, we focus on some special cases of global heat transfer, fluid friction, and magneto-resistive irreversibilities. For the global magneto-resistive irreversibility (GMRI), the role of Π^* has already been discussed. In the absence of any magnetic force (that is, $Ha_\delta=0$) the right-hand side of $(Ns_{av})_{MT}$ in Eq. (36) equals zero causing a zero contribution from GMRI which is, of course, desirable. From Eq. (36) one can show

$$\lim_{Ha_\delta\to\infty}(Ns_{av})_{MT}=0. \tag{39}$$

An increasing Hartmann number slows down the fluid motion near the stack and in the limit of an infinite Hartmann number the free stream velocity ($u_{1,\infty}$) becomes zero causing a zero contribution from the GMRI again. For the same reason the global fluid friction irreversibility (GFFI) is zero at high Hartmann number limit. However, in the absence of a magnetic field GFFI takes the following form:

$$\lim_{Ha_\delta\to 0}(Ns_{av})_{FF}=\frac{1}{2u_0^2}\left(\frac{\nabla p_1}{\rho_m\omega}\right)^2. \tag{40}$$

Note that the term$\nabla p_1/\rho_m\omega$ in Eq. (40) represents an equivalent standing wave velocity (u_1^s) as used by Swift [2] and Ishikawa and Mee [17]. In the high Hartmann number limit the expression for global heat transfer irreversibility (see Eq. (34)) takes the following forms:

$$\lim_{Ha_\delta\to\infty}(Ns_{av})_{HT}=\frac{\sqrt{Pr}}{2}\left(\frac{\beta p_1}{\rho_m C_p}\right)^2=\frac{\sqrt{Pr}}{2}\left(\frac{1}{T_m}\frac{T_m\beta p_1}{\rho_m C_p}\right)^2, \tag{41}$$

where the term $T_m\beta p_1/\rho_m C_p(=T_{ad})$ represents an expression for the fluctuating temperature due to an adiabatic oscillation in the absence of the stack (see Swift [2]). For a vanishingly small magnetic force ($Ha_\delta\to 0$) the global heat transfer irreversibility reduces to the following special form:

$$\begin{aligned}\lim_{Ha_\delta\to 0}(Ns_{av})_{HT}=&\frac{1}{2}\left(\frac{\nabla T_m}{T_m}\frac{\nabla p_1}{\rho_m\omega^2}\frac{Pr}{Pr-1}\right)^2\\&+\frac{\sqrt{Pr}}{2}\left(\frac{1}{T_m}\frac{\beta T_m p_1}{\rho_m C_p}+\frac{\nabla T_m}{T_m}\frac{\nabla p_1}{\rho_m\omega^2}\frac{1}{Pr-1}\right)^2\\&+\frac{\nabla T_m}{2T_m}\frac{\nabla p_1}{\rho_m\omega^2}\left\{\frac{1}{T_m}\frac{\beta T_m p_1}{\rho_m C_p}\frac{Pr}{Pr-1}\right.\\&\left.+\frac{\nabla T_m}{T_m}\frac{\nabla p_1}{\rho_m\omega^2}\frac{Pr}{(Pr-1)^2}\right\}\\&\times\left\{\frac{\sqrt{Pr}(1+\sqrt{Pr})}{1+Pr}+\frac{1}{T_m}\frac{\beta T_m p_1}{\rho_m C_p}\frac{1}{1+\sqrt{Pr}}\right\}\end{aligned} \tag{42}$$

where the term $\nabla p_1/\rho_m\omega^2$ represents the displacement amplitude. As the fluid oscillates along the direction of the stack with displacement amplitude $\nabla p_1/\rho_m\omega^2$, the temperature at a given point in space oscillates by an amount $\nabla T_m\nabla p_1/\rho_m\omega^2(=T_{sw})$ even if the temperature of a given piece of fluid remains constant. One can make an additional assumption; that is, $Pr\approx 1$ (for gas as working fluid) and obtain the following equation for the global heat transfer irreversibility

$$\begin{aligned}\lim_{\substack{Ha_\delta\to 0\\ Pr\to 1}}(Ns_{av})_{HT}=&\frac{1}{2}\left(\frac{\nabla T_m}{T_m}\frac{\nabla p_1}{\rho_m\omega^2}\right)^2\\&+\frac{1}{2}\left(\frac{1}{T_m}\frac{\beta T_m p_1}{\rho_m C_p}+\frac{1}{4}\frac{\nabla T_m}{T_m}\frac{\nabla p_1}{\rho_m\omega^2}\right)^2\\&+\frac{1}{2}\frac{\nabla T_m}{T_m}\frac{\nabla p_1}{\rho_m\omega^2}\left[\frac{1}{T_m}\frac{\beta T_m p_1}{\rho_m C_p}\right.\\&\times\left\{\frac{7}{4}+\frac{1}{2T_m}\frac{\beta T_m p_1}{\rho_m C_p}\right\}\\&\left.+\frac{11}{16}\frac{\nabla T_m}{T_m}\frac{\nabla p_1}{\rho_m\omega^2}\right].\end{aligned} \tag{43}$$

6.4. Local entropy generation

In order to assist interpretation, the time-averaged entropy generation rate (Ns_{tav} in Eq. (31)) is further subdivided into three parts: time-averaged entropy generation due to (a) heat transfer (Ns_{HT}), (b) fluid friction (Ns_{FF}), and (c) magnetic dissipation (Ns_{MT}), respectively. For selected drive ratio, frequency, Hartmann number, and temperature gradient, Ns_{HT}, Ns_{FF}, Ns_{MT}, and Ns_{tav} are plotted in Fig. 2 as a function of dimensionless transverse distance (y/δ_v). The variation in each of the entropy generation terms can be well understood if one recognizes their dependency on different parameters.

The magnetic dissipation contribution to entropy generation (Ns_{MT}) is proportional to the fluctuating velocity squared. Therefore, Ns_{MT} is zero at the wall due to the imposed no-slip boundary condition. Inside the boundary

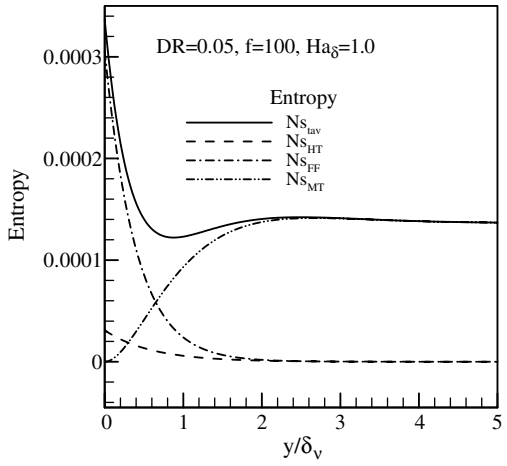

Fig. 2. Transverse variation in local entropy generation.

$$\frac{\partial T_1}{\partial y} = \left[-\frac{(1-i)\delta_v}{2} \frac{Pr}{\Psi_0^{3/2}} \frac{T_{sw}}{Pr-\Psi_0} \exp\left\{ -\frac{(1+i)\sqrt{\Psi_0}y}{\delta_v} \right\} \right] + \left[\frac{(1-i)\delta_k}{2} \left(T_{ad} + \frac{T_{sw}}{Pr-\Psi_0} \right) \exp\left\{ -\frac{(1+i)y}{\delta_k} \right\} \right] \tag{44}$$

where Ψ_0 equals $1 + Ha_\delta^2/2i$. An increasing Hartmann number has a general tendency to reduce both of the square bracketed terms in Eq. (44). On the other hand, an increasing ∇T_m has a general tendency to increase both of the square bracketed terms in Eq. (44) because T_{sw} is proportional to ∇T_m. The variation in Ns_{HT} with y/δ_v at different Hartmann numbers is shown in Fig. 3a for $\nabla T_m = 100$ and in Fig. 3b for $\nabla T_m = 10$, respectively. When $\nabla T_m = 100$ (Fig. 3a), a noticeable variation is observed in the Ns_{HT}–y/δ_v profiles with Hartmann number

layer Ns_{MT} shows a y-dependent variation which is a consequence of the variation in velocity inside the boundary layer. Outside the boundary layer Ns_{MT} shows asymptotic behavior where velocity (u_1) approaches a y-independent free stream velocity ($u_{1,\infty}$). The extent of the y-dependent Ns_{MT} largely depends on the Hartmann number. An increasing Hartmann number is responsible for a thinner boundary layer that causes a small layer of y-dependent Ns_{MT}. Therefore, in the limit of large Hartmann number $u_{1,\infty} \to 0$; there is no contribution from Ns_{MT} on the overall entropy generation rate (Ns_{tav}).

The fluid friction contribution to entropy generation (Ns_{FF}) is proportional to the fluctuating velocity gradient squared. Inside the boundary layer a velocity gradient exists which causes a nonzero Ns_{FF}. As the velocity gradient asymptotes to 0 and so does the Ns_{FF} outside the boundary layer. As u_1 approaches a constant and y-independent velocity ($u_{1,\infty}$) outside the boundary layer the corresponding velocity gradient approaches zero. Boundary layer thickness decreases with increasing Hartmann number and so does the extent of Ns_{FF}. Velocity gradient vanishes over the plate when $Ha_\delta \to \infty$, therefore, the contribution of Ns_{FF} on overall entropy generation rate at high Hartmann number is insignificant.

The heat transfer contribution to entropy generation (Ns_{HT}) is proportional to the fluctuating temperature gradient squared. The variation of T_1 inside the boundary layer causes a finite variation in Ns_{HT}. As T_1 approaches a constant and y-independent temperature ($T_{1,\infty}$) outside the boundary layer the corresponding temperature gradient approaches zero; that is, the contribution of Ns_{HT} to overall entropy generation is insignificant outside of the boundary layer. The complicated appearance of the Hartmann number (Ha_δ) and temperature gradient (∇T_m) in Eq. (24) introduces additional difficulties in interpreting the functional relationship among Ns_{HT}, Ha_δ , and ∇T_m. The fluctuating temperature gradient, $\partial T_1/\partial y$, is calculated from Eq. (24) and presented in the following equation:

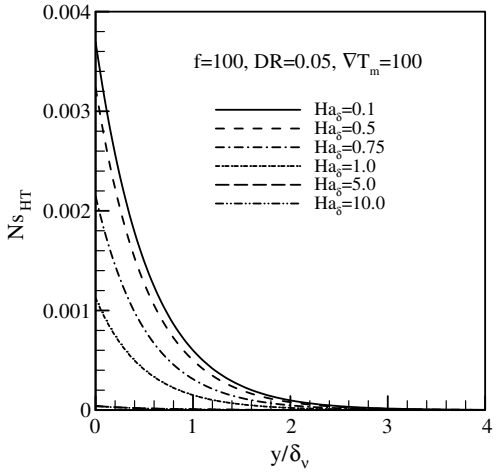

Fig. 3a. Transverse variation in local heat transfer irreversibility at $\nabla T_m = 100$.

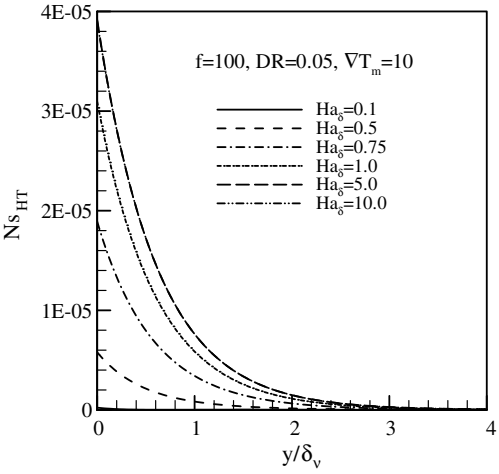

Fig. 3b. Transverse variation in local heat transfer irreversibility at $\nabla T_m = 10$.

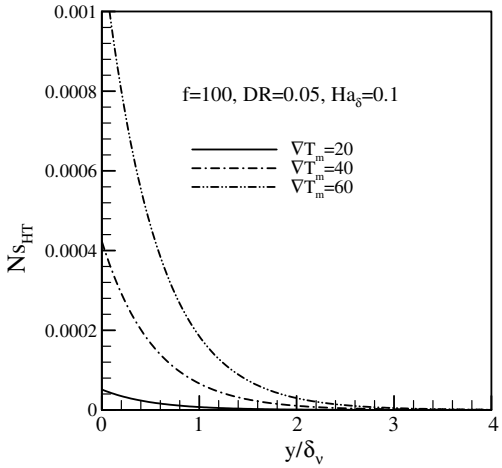

Fig. 3c. Transverse variation in local heat transfer irreversibility at $Ha_\delta = 0.1$.

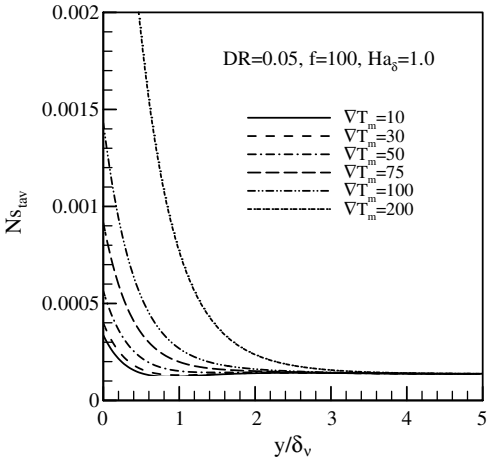

Fig. 4a. Time-averaged entropy generation at different ∇T_m.

variation. An increasing Hartmann number reduces the magnitude of Ns_{HT}. However, when $\nabla T_m = 10$ (Fig. 3b), the variation in Ns_{HT} is very small while an increasing Hartmann number increases the magnitude of Ns_{HT}. Similarly, the influence of ∇T_m on Ns_{HT} is shown in Fig. 3c and 3d. For a low Hartmann number (for example, $Ha_\delta = 0.1$) an increase in ∇T_m increases Ns_{HT} as shown in Fig. 3c. However, the variation in Ns_{HT} with ∇T_m at high Hartmann number is insignificant (Fig. 3d).

The time-averaged local entropy generation rate (Ns_{tav}) is the sum of Ns_{HT}, Ns_{FF}, and Ns_{MT}. Both Ns_{HT} and Ns_{FF} decrease with increasing transverse distance and approach zero outside the boundary layer while Ns_{MT} increases from zero with increasing transverse distance and approaches a constant value outside the boundary layer. In Fig. 4a, Ns_{tav} is plotted as a function of transverse distance at different ∇T_m. The nature of the variation in each Ns_{tav} profile can be understood from the preceding discussions. As we consider a constant Hartmann number in Fig. 4a, the Ns_{tav}–y/δ_v profiles merge with each other outside the boundary layer where Ns_{tav} equals Ns_{MT} only. It is already seen that the Ns_{MT} and Ns_{FF} are independent of ∇T_m's variation. Therefore, inside the boundary layer, Ns_{tav} increases with an increase in ∇T_m. Bejan number, a measure of heat transfer irreversibility, is a ratio of entropy generation due to heat transfer to the overall entropy generation rate. The time-averaged Bejan number (Be_{tav}) is plotted in Fig. 4b at different ∇T_ms. Although Ns_{HT} is maximum at the wall; Be_{tav} profiles show their maximum value near the wall where Ns_{tav}s shows its local minimum due to opposite behavior of Ns_{FF} and Ns_{MT} with y/δ_v. Outside the boundary layer, Ns_{HT} approaches zero and so does the Bejan number.

6.5. Global entropy generation

We have already presented and discussed some limiting cases of global entropy generation rates. Additional graphical results are presented in this section in order to understand the influence of different parameters (for example,

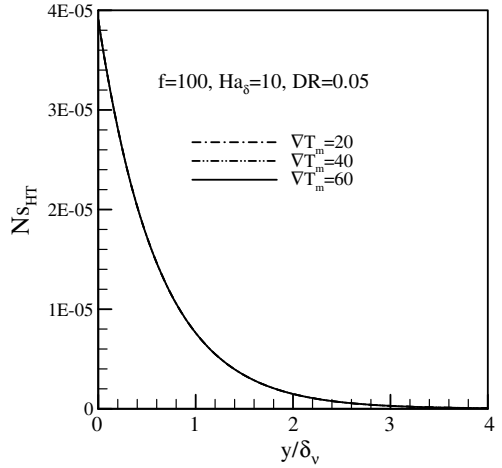

Fig. 3d. Transverse variation in local heat transfer irreversibility at $Ha_\delta = 10.0$.

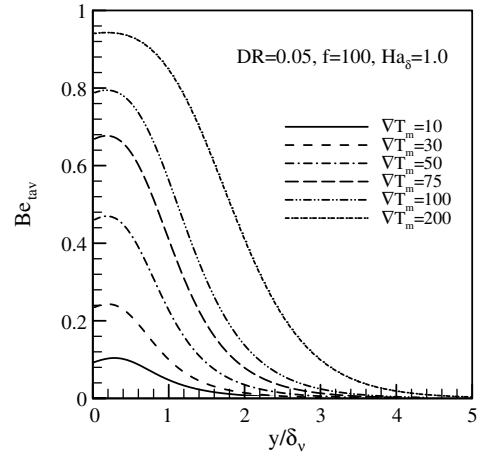

Fig. 4b. Time-averaged Bejan number at different ∇T_m.

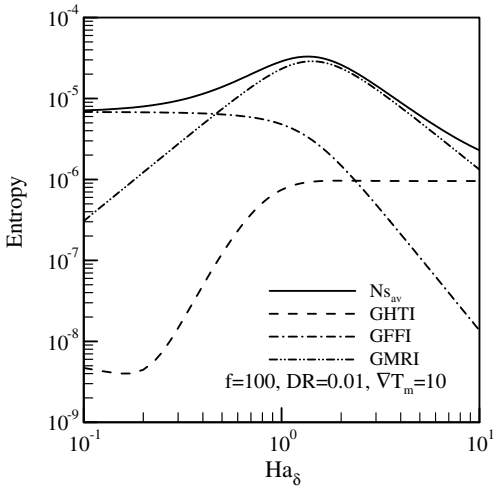

Fig. 5a. GHTI, GFFI, GMTI, and Ns_{av} as a function of Hartmann number at $\nabla T_m = 10$.

drive ratio, frequency, Hartmann number, etc.) on global entropy generation rate (Ns_{av}). It has already been shown that the global entropy generation rate or the global thermoacoustic irreversibility is the sum of GHTI (see Eq. (34)), GFFI (see Eq. (35)), and GMRI (see Eq. (36)). In order to understand the variation of Ns_{av}, one requires understanding of the individual variation of GHTI, GFFI, and GMRI. For two selected cases, Figs. 5a and 5b show the variation of Ns_{av}, GHTI, GFFI, and GMRI as a function of Hartmann number.

Consider the variation of GMRI. For the selected range of Hartmann number, GMRI increases with increasing Hartmann number (Figs. 5a and 5b), shows a maximum at $Ha_\delta \approx 1.0$, and then decreases with further increases in Hartmann number. It has already been shown that for two limiting cases of Hartmann number ($Ha_\delta \to 0$ and $Ha_\delta \to \infty$) GMRI approaches to zero. This trend is supported by the decreasing tendency of GMRI with decreasing Ha_δ when $Ha_\delta < 1.0$ and increasing Ha_δ when $Ha_\delta > 1.0$ as shown in Figs. 5a and 5b. When $Ha_\delta > 1$, the Lorentz force dominates the viscous force. An increasing Hartmann number introduces a drag effect in the flow field (Mahmud and Fraser [12]) and consequently it reduces the velocity and the GMRI. The $u_{1,\infty}, \tilde{u}_{1,\infty}$ term in Eq. (36) is inversely proportional to $1 + Ha_\delta^4/4$. Therefore, an increasing Hartmann number (when $Ha_\delta > 1$) rapidly reduces $u_{1,\infty}, \tilde{u}_{1,\infty}$, and in the limit of large Hartmann number $u_{1,\infty}, \tilde{u}_{1,\infty}$ approaches zero. When $Ha_\delta < 1$, the viscous force dominates the Lorentz force. For such a situation a decreasing Hartmann number does not show a significant effect on the flow field. Close observation of the terms outside the square bracket of Eq. (36) reveals that any decrease in Hartmann number (when $Ha_\delta < 1$) reduces the GMRI and in the limit of vanishing Hartmann number GMRI approaches zero.

Next, consider the variation of GFFI. As the influence of Hartmann number is small on the flow field when $Ha_\delta < 1$, GFFI shows little variation with Hartmann number variation. When $Ha_\delta > 1$, an increasing Hartmann number reduces the extent of the shear layer and, as a consequence, reduces the global fluid friction irreversibility. In the limit of large Hartmann number GFFI is zero.

The variation of GHTI can be well understood if one understands its local distribution (Fig. 3) and the influence of ∇T_m and Ha_δ on it. The transverse distribution of Ns_{HT} shows different characteristics at high and low temperature gradients (see Figs. 3a and 3b). An increasing ∇T_m has a general tendency to increase $\partial T_1/\partial y$ (so does an increasing Ns_{HT}), while an increasing Ha_δ generally decreases $\partial T_1/\partial y$ (so does an increasing Ns_{HT}). Therefore, for a given range of Hartmann number, the GHTI–Ha_δ plot shows opposite behavior at low and high ∇T_ms as shown in Figs. 5a and 5b.

The distribution pattern of the global thermoacoustic irreversibility (Ns_{av}) is greatly influenced by GHTI as shown in Figs. 5a and 5b. Fig. 6a shows the distribution

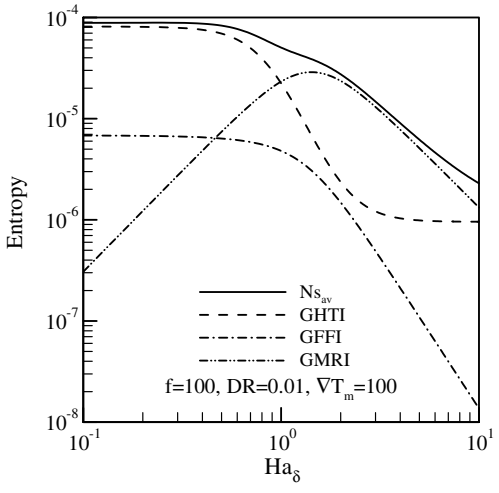

Fig. 5b. GHTI, GFFI, GMTI, and Ns_{av} as a function of Hartmann number at $\nabla T_m = 100$.

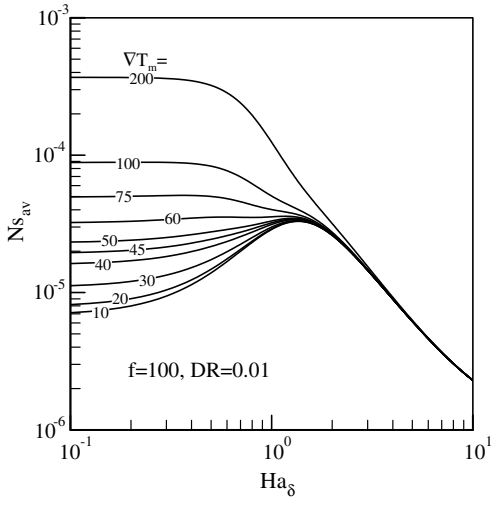

Fig. 6a. Average entropy generation as a function of Hartmann number at different ∇T_m.

of Ns_{av} as a function of Ha_δ at different ∇T_ms. When $Ha_\delta < 1$, the magnitude of Ns_{av} shows a considerable variation with changes in ∇T_m. However, this variation is insignificant when $Ha_\delta > 1$. Now, observe the Ns_{av}–Ha_δ profiles when $\nabla T_m < 60$ and $\nabla T_m > 60$, respectively. When $\nabla T_m < 60$ the maximum Ns_{av} occurs near $Ha_\delta \approx 1.0$ and no distinct maximum exists when $\nabla T_m > 60$. In order to understand this behavior one needs to calculate the critical temperature gradient (∇T_{cr}) from Eq. (A1). One can set the fluid properties, temperature gradient, and flow properties in such a way that both terms on the right-hand side of Eq. (A1) become equal resulting in $T_{1,\infty} \approx 0$. In such a case, the resulting temperature gradient is a critical temperature gradient (∇T_{cr}) that can be estimated from

$$\nabla T_{cr} = \frac{1}{4}\left[\frac{T_m \beta p_1}{\rho_m C_p}\right]\left[\frac{\omega^2 \rho_m}{\nabla p_1}\right](1 + Ha_\delta^4) \tag{45}$$

for the present problem. Note that the terms inside the first square bracket is the adiabatic temperature oscillation and inside the second square bracket is the inverse of the displacement amplitude. The critical temperature gradient plays a key role in determining the mode of operation (prime mover or heat pump mode) for a particular thermoacoustic engine. For an inviscid single-plate thermoacoustic system, Swift [2] calculates a critical temperature gradient which results in zero heat flux and work flux; that is, effectively no thermoacoustic effect. Swift's [2] single-plate thermoacoustic device works as a prime mover when $\nabla T_m > \nabla T_{cr}$ and as a heat pump when $\nabla T_m < \nabla T_{cr}$, respectively. In the presence of viscosity, longitudinal thermal conductivity, magnetic force, etc., the definition of the critical temperature gradient becomes more complicated. For the current set of parameters $\nabla T_{cr} \approx 62$; this acts as the limiting value for a particular mode of operation. A distinct maximum in Ns_{av} is observed only when $\nabla T_m < \nabla T_{cr}$.

Average Bejan number (Be_{av}) is plotted in Fig. 6b as a function of Hartmann number at different ∇T_ms. When Hartmann number is small, the GHTI and GFFI show very small variations with Hartmann number variation. On the contrary, the GMRI increases with increasing Hartmann number when $Ha_\delta < 1$ which in turn causes a reduction in Bejan number with increasing Hartmann number for all ∇T_m shown in Fig. 6b except $\nabla T_m = 10$. However, when Hartmann number is large, the GFFI and GMRI decrease with increasing Hartmann number, but the GHTI is insensitive to the Hartmann number variation which in turn causes an increase in Bejan number with increasing Hartmann number. These opposite trends in the Be_{av}–Ha_δ profile at low and high Hartmann number are responsible for the minimum Be_{av} that occurs near $Ha_\delta \approx 1.0$.

For a constant ∇T_m the effect of the drive ratio on the global thermoacoustic irreversibility is shown in Fig. 6c. Close observation of Eqs. (34)–(36) reveals that the pressure and pressure gradient terms are directly proportional to GHTI, GFFI, and GMRI. Therefore, an increase in the drive ratio increases the global thermoacoustic irreversibility as shown in Fig. 6c.

The effect of frequency variation on Ns_{av} is shown in Fig. 6d. A change in frequency affects the particle displacement length (d_p) and the viscous and thermal penetration depths (δ_v,δ_k) according to

$$d_p \sim \frac{1}{f} \text{ and} (\delta_v, \delta_k) \sim \frac{1}{\sqrt{f}}. \tag{46}$$

A higher frequency reduces the particle displacement length and the viscous and thermal penetration depths, thus resulting in a thinner region over the stack in which the thermoacoustic phenomenon is in effect. Therefore, an increasing frequency shows a decrease in the global thermoacoustic irreversibility when $Ha_\delta < 1.0$. However, the effect of frequency change on Ns_{av} is insignificant when $Ha_\delta > 1.0$. The following relationships help one to understand the functional relationship of frequency with GFFI, and GMRI:

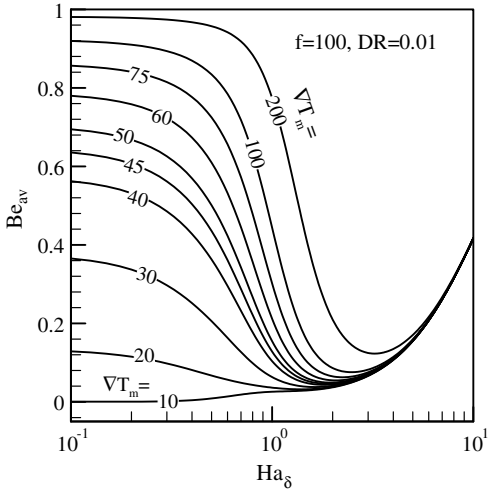

Fig. 6b. Average Bejan number as a function of Hartmann number at different ∇T_m.

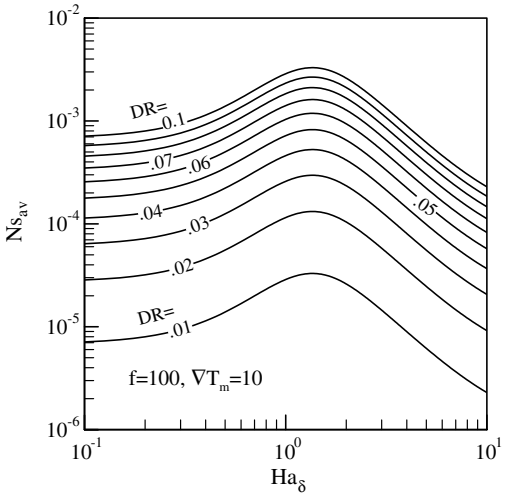

Fig. 6c. Average entropy generation as a function of Hartmann number at different drive ratio.

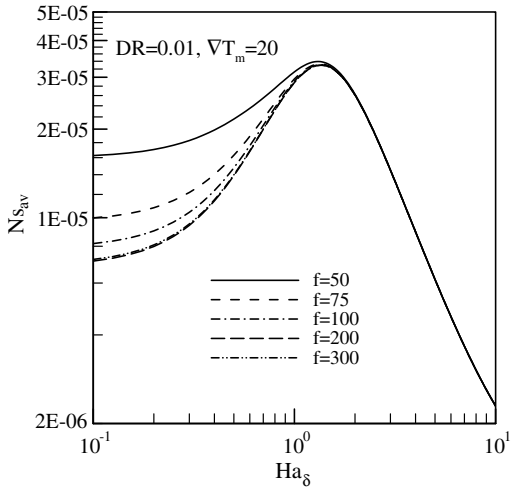

Fig. 6d. Average entropy generation as a function of Hartmann number at different frequency.

$$\sqrt{u_{1,\infty}\tilde{u}_{1,\infty}} \sim \frac{\nabla p_1}{\omega} \text{ where } \nabla p_1 \sim \frac{1}{\lambda} \sim f \text{ and } \omega \sim f. \qquad (47)$$

Both GFFI (Eq. (35)) and GMRI (Eq. (36)) are proportional to the product of $u_{1,\infty}$, and $\tilde{u}_{1,\infty}$, and each of these terms has a functional relationship with frequency. However, their product $(u_{1,\infty}\tilde{u}_{1,\infty})$ is independent of frequency variation (see Eq. (47)) which results in GFFI and GMRI variations being independent of frequency variation. Both the b_1 and b_2 terms and their complex conjugates (see Eq. (34) and Eqs. (A5) and (A6)) have non-vanishing frequency. Therefore, the frequency variation of the global thermoacoustic irreversibility (Ns_{av}) solely depends on the frequency variation in GHTI.

7. Conclusions

The aim of the current research effort is to incorporate into the existing thermoacoustic theory a modification that uses a magnetic force as a non-contact thermoacoustic effect controlling mechanism, and to analyze the irreversibility of a single plate thermoacoustic engine in the presence of a magnetic force. In the limit of large transverse distance ($y \to \infty$), the fluctuating velocity (u_1) and temperature (T_1) approach the y-independent free stream velocity ($u_{1,\infty}$) and temperature ($T_{1,\infty}$), respectively. In reality, this 'large transverse distance' is limited to a few δ_v or δ_k (that is, the viscous and thermal penetration depths). It is possible to divide the global thermoacoustic irreversibility into three parts: (a) global magneto-resistive irreversibility (GMRI), (b) global fluid friction irreversibility (GFFI), and (c) global heat transfer irreversibility (GHTI). For two limiting cases of Hartmann number ($Ha_\delta \to 0$ and $Ha_\delta \to \infty$), GMRI approaches zero. GMRI shows its maximum value near $Ha_\delta \approx 1$ while GFFI is zero only when $Ha_\delta \to \infty$, however, GHTI is nonzero at these two limiting cases of the Hartmann number. The GHTI (which is influenced by variation in ∇T_m and Ha_δ) influences greatly the distribution pattern of the global thermoacoustic irreversibility (Ns_{av}). The critical temperature gradient (∇T_{cr}) plays an important role for determining the local Ns_{av} maximum. Increasing drive ratio increases the global thermoacoustic irreversibility while increasing frequency decreases the global thermoacoustic irreversibility when $Ha_\delta < 1.0$.

Appendix

$$T_{1,\infty} = \frac{\beta T_m p_1}{\rho_m C_p} - \frac{\nabla T_m \nabla p_1}{\omega^2 \rho_m (1 - iHa_\delta^2/2)},$$

$$\tilde{T}_{1,\infty} = \frac{\beta T_m p_1}{\rho_m C_p} - \frac{\nabla T_m \nabla p_1}{\omega^2 \rho_m (1 + iHa_\delta^2/2)}, \qquad (A1)$$

$$u_{1,\infty} = \frac{i}{\rho_m \omega}\left(1 + \frac{i}{2}Ha_\delta^2\right)\left(1 + \frac{1}{4}Ha_\delta^4\right)^{-1}\frac{\partial p_1}{\partial x},$$

$$\tilde{u}_{1,\infty} = -\frac{i}{\rho_m \omega}\left(1 - \frac{i}{2}Ha_\delta^2\right)\left(1 + \frac{1}{4}Ha_\delta^4\right)^{-1}\frac{\partial p_1}{\partial x}, \qquad (A2)$$

$$a_0 = \frac{1+i}{\delta_v}\sqrt{1 - \frac{iHa_\delta^2}{2}} = \frac{1+i}{\sqrt{\mathrm{Pr}}\delta_k}\sqrt{1 - \frac{iHa_\delta^2}{2}},$$

$$\tilde{a}_0 = \frac{1-i}{\delta_v}\sqrt{1 + \frac{iHa_\delta^2}{2}} = \frac{1-i}{\sqrt{\mathrm{Pr}}\delta_k}\sqrt{1 + \frac{iHa_\delta^2}{2}}, \qquad (A3)$$

$$b_0 = \frac{1+i}{\delta_k} = \frac{1+i}{\delta_v}\sqrt{\mathrm{Pr}}, \quad \tilde{b}_0 = \frac{1-i}{\delta_k} = \frac{1-i}{\delta_v}\sqrt{\mathrm{Pr}}, \qquad (A4)$$

$$b_1 = \frac{\nabla T_m \nabla p_1}{\omega^2 \rho_m (1 - iHa_\delta^2/2)}\frac{\mathrm{Pr}}{\mathrm{Pr} - (1 - iHa_\delta^2/2)},$$

$$\tilde{b}_1 = \frac{\nabla T_m \nabla p_1}{\omega^2 \rho_m (1 + iHa_\delta^2/2)}\frac{\mathrm{Pr}}{\mathrm{Pr} - (1 + iHa_\delta^2/2)}, \qquad (A5)$$

$$b_2 = \frac{\beta T_m p_1}{\rho_m C_p} + \frac{\nabla T_m \nabla p_1}{\omega^2 \rho_m}\frac{1}{\mathrm{Pr} - (1 - iHa_\delta^2/2)},$$

$$\tilde{b}_2 = \frac{\beta T_m p_1}{\rho_m C_p} + \frac{\nabla T_m \nabla p_1}{\omega^2 \rho_m}\frac{1}{\mathrm{Pr} - (1 + iHa_\delta^2/2)}. \qquad (A6)$$

References

[1] N. Rott, Thermoacoustics, Adv. Appl. Mech. 20 (1980) 135–175.
[2] G.W. Swift, Thermoacoustic engines, J. Acous. Soc. Am. 84 (1988) 1145–1180.
[3] K.T. Feldman, Review of the literature of Rijke thermoacoustic phenomena, J. Sound Vib. 7 (1968) 83–89.
[4] G. Kirchhoff, Über den Einfluss der Wärmeleitung in einem Gas auf die Schallbewegung, Annu. Phys. (Leipzig) 134 (1868) 177–193.
[5] L. Rayleigh, The Theory of Sound, Dover, New York, 1945.
[6] G.W. Swift, Thermoacoustics: An Unifying Perspective for Some Engines and Refrigerators, ASA Publication, New York, 2002.
[7] R. Raspet, H.E. Bass, J. Kordomenos, Thermoacoustic of travelling waves: theoretical analysis for an inviscid ideal gas, J. Acous. Soc. Am. 94 (1993) 2232–2239.
[8] A.O. Santillan, R.R. Boullosa, Space dependence of acoustic power and heat flux in the thermoacoustic effect, Int. Commun. Heat Mass Transfer 22 (1995) 539–548.

[9] A.O. Santillan, R.R. Boullosa, Acoustic power and heat flux in the thermoacoustic effect due to travelling plane wave, Int. J. Heat Mass Transfer 40 (1997) 1835–1838.
[10] G.W. Swift, A. Migliori, T. Hofler, J. Wheatley, Theory and calculations for an intrinsically irreversible acoustic prime mover, J. Acous. Soc. Am. 78 (1985) 767–781.
[11] J.C. Wheatley, G.W. Swift, A. Migliori, The Natural Heat Engine, Los Alamos Science, 1986, pp. 2–29.
[12] S. Mahmud, R.A. Fraser, Magnetohydrodynamic free convection and entropy generation in a square porous cavity, Int. J. Heat Mass Transfer 47 (2004) 3245–3256.
[13] B.R. Gopal, R. Chahine, M. Foldeaki, T.K. Bose, Noncontact thermoacoustic method to measure the magnetocaloric effect, Rev. Sci. Instrum. 66 (1995) 232–238.
[14] G. Ibanez, S. Cuevas, M.L. de Haro, Optimization analysis of an alternate magnetohydrodynamic generator, Energy Conver. Manag. 43 (2002) 1757–1771.
[15] G. Ovando, G. Huelsz, E. Ramos, S. Cuevas, Effect of magnetic field on the linear stability of a thermoacoustic oscillation, J. Non-Equilib. Thremodyn. 30 (2005) 137–149.
[16] E. Besnoin, O.M. Knio, Numerical study of thermoacoustic heat exchangers in the thin plate limit, Num. Heat Transfer (Part A) 40 (2001) 445–471.
[17] H. Ishikawa, D.J. Mee, Numerical investigation of flow and energy fields near a thermoacoustic couple, J. Acous. Soc. Am. 111 (2002) 831–839.
[18] A. Bejan, Entropy Generation Minimization, CRC Press, New York, 1996.
[19] A. Bejan, Fundamental of exergy analysis, entropy generation minimization and the generation of flow architecture, Int. J. Energy Res. 26 (2002) 545–565.
[20] R.B. Bird, W.E. Stewart, E.N. Lightfoot, Transport Phenomena, Wiley, New York, 2002.
[21] M.F. Romig, The influence of electric and magnetic fields on heat transfer to electrically conducting fluids, Adv. Heat Transfer 1 (1964) 267–354.
[22] U. Müller, L. Bühler, Magnetofluiddynamics in Channel and Containers, Springer-Verlag, Berlin, 2002.
[23] L.C. Burmeister, Convective Heat Transfer, Wiley, New York, 1993.
[24] A. Bejan, Convection Heat Transfer, Wiley, New York, 1984.
[25] P.A. Davidson, An Introduction to Magnetohydrodynamics, Cambridge University Press, Cambridge, 2001.
[26] R. Viskanta, Electric and magnetic fields, in: W.M. Rohsenow, J.P. Hartnett, E.N. Ganić (Eds.), Handbook of Heat Transfer Fundamentals, McGraw-Hill, New York, 1985 (Chapter 10).
[27] S. Mahmud, R.A. Fraser, The second law analysis in fundamental convective heat transfer problems, Int. J. Thermal Sci. 42 (2003) 177–186.
[28] S. Temkin, Elements of Acoustics, Wiley, New York, 1981.
[29] S. Mahmud, R.A. Fraser, Flow and heat transfer inside porous stack: steady-state problem, Int. Com. Heat Mass Transfer 31 (2004) 951–962.